https://doi.org/10.5194/acp-2019-634
Preprint. Discussion started: 16 September 2019

Atmospheric Chemistry and Physics Discussions

Elucidating the ozone pollution in Yangtze River Delta region during the 2016 G20 summit for MICS-Asia III

Zhi-zhen Ni[1], Kun Luo[1*], Yang Gao[2], Xiang Gao[1], Fei Jiang[3], Huang Cheng[4], Jian-ren Fan[1], Joshua S. Fu[5], Chang-hong Chen[4]

[1]State Key Laboratory of Clean Energy, Department of Energy Engineering, Zhejiang University, Hangzhou 310027, China

[2] Key Laboratory of Marine Environment and Ecology, Ministry of Education of China, Ocean University of China, Qingdao 266100, China

[3]International Institute for Earth System Science, Nanjing University, Nanjing, China

[4]Shanghai Academy of Environmental Sciences, Shanghai 200233, China

[5]Civil & Environmental Engineering, the University of Tennessee, Neyland, UK

[*]Correspondence to: zjulk@zju.edu.cn

https://doi.org/10.5194/acp-2019-634
Preprint. Discussion started: 16 September 2019

Atmospheric Chemistry and Physics Discussions

Abstract

To elucidate the factors governing urban ozone (O_3) pollution during the campaign of G20 summit in 2016 Hangzhou, China, the Weather Research Forecast with Chemistry (WRF-Chem) model was used to simulate the spatial and temporal O_3 evolution in the Yangtze River Delta (YRD) region from 24 August to 06 September 2016. Various atmospheric processes were analyzed to determine the influential factors of ozone formation through integrated process rate method. The results indicated that both the vertical diffusion and the enhanced process of local chemical generation accounted for the increase of surface O_3 concentration in Hangzhou. Local chemical generation was found to positively correlated with O_3 concentrations, with correlation coefficient of 0.77. In accordance with the tropical weather cycle, subsidence air and stagnant weather were induced. Dynamic circulations of O_3 through advection were associated with the urban heat island effect. All these factors intensified ozone pollution in Hangzhou, particularly on 25 August 2016 (O_3-8h: 98 ppb). These findings provide insight into urban O_3 formation and dispersion during tropical cyclone events, and support the Model Intercomparison Study Asia Phase III (MICS-Asia Phase III).

Keywords: Ozone, Tropical cyclone, WRF-Chem, Process analysis, Air quality

https://doi.org/10.5194/acp-2019-634
Preprint. Discussion started: 16 September 2019

1. Introduction

Tropospheric ozone (O_3) is generated by a series of photochemical reactions involving volatile organic compounds (VOCs), nitrogen oxide (NO_x), and carbon monoxide (CO) (Wang et al., 2006). As a primary component of photochemical smog, ground-level O_3 pollution exhibits detrimental effects on human health (Ha et al., 2014; Kheirbek et al., 2013) and the ecosystem (Landry et al., 2013; Teixeira et al., 2011). The contribution of outdoor air pollution sources to premature mortality may increase globally in the coming decades (Lelieveld et al., 2015). O_3 levels in cities in the United States and Europe are increasing more than those in the rural areas of these regions, where peak values decreased during 1990–2010 (Paoletti et al., 2014). Nagashima et al., (2017) reported that long-term (1980 – 2005) trends of increase in surface O_3 over Japan may be primarily attributed to the continental transport that have contributed to photochemical O_3 production. Urban O_3 pollution events can also be observed in developing countries, such as Thailand (Zhang and Kim Oanh, 2002) and India (Calfapietra et al., 2016).

Air quality has been deteriorating in China as urbanization and motorization have progressed. Many field and modeling studies have investigated the photochemical characteristics of near-surface O_3 (Tang et al., 2009, 2012; Wang et al., 2013, 2014), the photochemistry of O_3 and its precursors (Xie et al., 2014), interactions of O_3 with $PM_{2.5}$ (Shi et al., 2015), and urban O_3 formation (Tie et al., 2013). In addition to anthropogenic emissions of O_3 precursors, uncontrollable physical and chemical processes involved in meteorological phenomena critically modulate changes in O_3 concentration (Xue et al., 2014). In the Yangtze River Delta (YRD) region of China, high O_3 concentrations are associated with pollutant transport and diffusion from surrounding areas (Gao et al., 2016; Jiang et al., 2012). Synoptic patterns related to tropical cyclones may be conducive to high O_3 concentrations (Huang et al., 2005). Jiang et al. (2015) reported that enhanced stratosphere – troposphere exchange (STE) driven by a tropical cyclone abruptly increased O_3 concentrations (21 – 42 ppb) in the southeast of China during June 12 – 14, 2014. STE has been highlighted as a significant contributor to near-surface O_3 concentrations (Lin et al., 2012, 2015).

https://doi.org/10.5194/acp-2019-634
Preprint. Discussion started: 16 September 2019

Because relevant data are limited, the complex dynamics in atmospheric processes related to O_3 formation are difficult to evaluate, and the main processes that account for high O_3 concentrations are challenging to identify. O_3 pollution characteristics and underlying causes have not been sufficiently investigated in China, especially in relation to extreme meteorological conditions. The lack of relevant data may influence urban pollution prevention efforts.

In this study, a regional air quality model, within the framework of the Model Inter-Comparison Study for ASIA phase III (MICS-ASIA III) (Li et al., 2019), was used to elucidate the chemical and physical factors that contributed to O_3 abundance during the G20 (Group of Twenty) summit. The summit was held in Hangzhou, China, and the focus of the summit was the sustainable and healthy development of the world economy. Emergency emission control measures (e.g., industrial stoppages, limitations of vehicle movement) were implemented over an area with a diameter of approximately 600 km to improve the air quality from 24 August to 06 September 2016. Because of severe concerns regarding O_3 concentrations and the summer cyclonic weather pattern, the aforementioned pollution control event attracted wide policy-related interest. The rest of this paper is organized as follows. Section 2 outlines the methodology and configuration of the model system. Section 3 describes the synoptic weather conditions as well as individual O_3 formation–related atmospheric processes. Section 4 discusses causes of O_3 pollution. Finally, section 5 presents a summary of the findings.

2. Methodology

2.1. Regional chemistry modeling system

To investigate the interactions among emissions, meteorological phenomena, and chemical phenomena, the Weather Research Forecast with Chemistry model (WRF-Chem) was used to simulate temporal and spatial changes in O_3 concentration. WRF-Chem is a regional online-coupled air quality model that simultaneously simulates air quality components and meteorological components by using identical transport schemes, grid structures, and physical schemes (Grell et al., 2005). Two model domains were designed in this study (Fig. 1a): an outer domain (horizontal

https://doi.org/10.5194/acp-2019-634
Preprint. Discussion started: 16 September 2019

resolution: 30 km) covering East China (20.0 °N – 44.5 °N, 99.0 °E – 126.5 °E) and an inner domain (horizontal resolution: 6 km) covering the YRD region (27.6 °N – 32.7 °N, 116.9 °E – 122.4 °E). The "Lambert conformal conic" projection was applied with domain center at 34 °N, 111 °E. There is a total of 31 vertical layers with model top at 50 hPa. The simulation period was from 17 August to 06 September 2016, and simulations of the first week were used to spin up the model. Hourly model outputs for 24 August to 06 September were used in the analysis. Additional details regarding the configuration of the WRF-Chem model are described in our previous study (Ni et al., 2018).

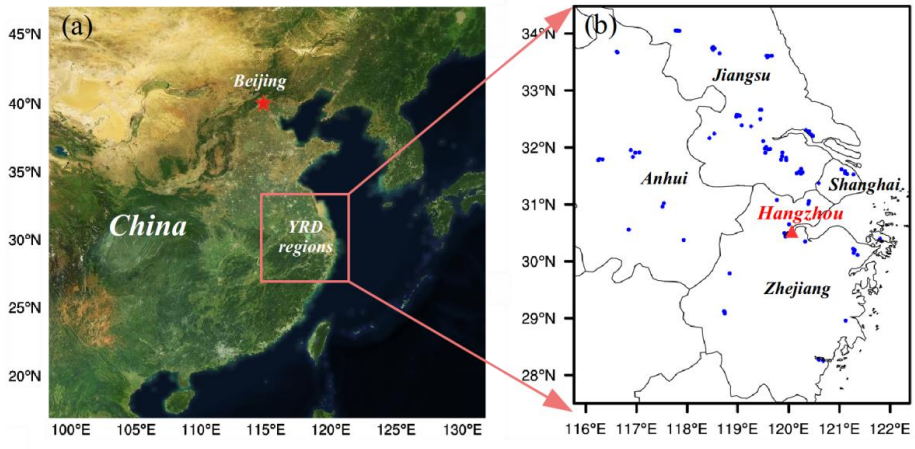

Fig. 1. Double-nested simulation domains. (a) Domain 1: 30 km in East China with 102 (W – E) × 111 (S – N) × 31 (vertical layers) grids. The copyright of map is own to © Google; (b) Domain 2: 6 km in the Yangtze River Delta (YRD) region with 100 (W – E) × 115 (S – N) × 31 (vertical layers) grids. Blue dots denote the air quality monitoring sites.

The meteorological boundary and initial conditions were determined from the global objective final analysis (FNL) data of the National Centers for Environmental Prediction (Kalnay et al., 1996). The FNL data were also assimilated to domain 1 (East China), and the grid-nudging method (Stauffer et al., 1991) was used to reduce the meteorological integral errors. The chemical initial and boundary conditions were dynamically downscaled from the model for ozone and related chemical tracers, version 4 (MOZART4) (Emmons et al., 2010) simulation results; the relevant data are available at https://www.acom.ucar.edu/wrf-chem/mozart.shtml.

https://doi.org/10.5194/acp-2019-634
Preprint. Discussion started: 16 September 2019

2.2. Emissions

The 2016 Multiresolution Emission Inventory for China (MEIC, 0.25° × 0.25°; http://www.meicmodel.org/) was used for the outer domain (Fig. 1a) with spatial resolution of 30 km (Li et al., 2017), including species of SO_2, NO_x, CO, NH_3, $PM_{2.5}$, and VOCs from the power, industrial, residential, transportation, and agricultural sectors. Inventories of finer anthropogenic emissions for the YRD region (Fig. 1b) over the year of 2014 were compiled based on the bottom-up method by Shanghai Academy of Environmental Sciences. These inventories have been documented in detail in previous studies (Huang et al., 2011; Li et al., 2011; Liu et al., 2018). Thus, only brief discussions of these inventories are presented herein. The fine emission inventories include major sectors such as large point sources, industrial sources, mobile sources, and residential sources. The anthropogenic emissions over the YRD region are mainly located over the industrial and urban areas along the Yangtze River as well as over Hangzhou Bay. In this study, the emission inventories for the two domains were projected into horizontal and vertical grids as hourly emissions, with temporal and vertical profiles obtained from Wang et al. (2011). VOCs emissions were categorized into modeled species, according to von Schneidemesser et al. (2016). In addition, biogenic emissions were generated offline using the Model of Emission of Gases and Aerosols from Nature (MEGAN) (Guenther et al., 2006). Dust emissions were calculated online from surface features and meteorological fields by using the Air Force Weather Agency and Atmospheric and Environmental Research scheme (Jones et al., 2011). Other emissions (i.e., those from biomass burning, aviation, and sailing ships), accounting for very small fractions during this period, were therefore not considered in this study.

2.3. Atmospheric processes analysis

To understand the mechanism underlying O_3 formation, individual physical and chemical processes of O_3 formation were investigated using integrated process rate (IPR) analysis in the WRF-Chem model. IPR analysis has been widely applied; this method has been proven to be an effective tool for demonstrating the relative importance of individual processes and for interpreting

https://doi.org/10.5194/acp-2019-634
Preprint. Discussion started: 16 September 2019

O_3 concentrations (Goncalves et al., 2009; Tang et al., 2017; Shu et al., 2016). The present study investigated atmospheric processes involved in O_3 formation, including gas chemistry, vertical diffusion, and horizontal and vertical advection. Other processes (i.e., cloud processes and horizontal diffusion) that either play minor roles or result in the formation of a sink (i.e., dry and wet deposition) were not considered in this study.

2.4. Evaluation method

To increase the confidence in interpretations of model results, model outputs should first be evaluated based on observations. Accordingly, in this study, the model results derived from domain 2 were compared with hourly surface observational data obtained from 96 air quality monitoring sites in the YRD region (blue dots, Fig. 1b). These data were downloaded from http://www.pm25.in. The air pollutants assessed were O_3 and NO_2. Model performance was evaluated using statistical measures, namely mean fractional bias (MFB), mean fractional error (MFE), and correlation coefficient (R), following the recommendation of the US Environmental Protection Agency (US EPA; 2007). The formula used in this evaluation is presented in Table S1. Additionally, the meteorological parameters were evaluated based on observational data—including temperature at 2 m (T2), relative humidity at 2 m (RH2), and 10 m wind speed (WS10) and direction (WD10)—from the Meteorological Assimilation Data Ingest System (https://madis.noaa.gov). Following the study of Zhang et al. (2014), commonly used mean bias (MB), gross error (GE), and root mean square error (RMSE) were calculated as the statistical indicators; corresponding equations are denoted in Table S1.

The vertical distribution of modeled O_3 in Hangzhou was evaluated based on comparisons with observed differential absorption LiDAR (DIAL) data (Su et al. 2017). In the DIAL technique, the mean gas concentration over a certain range interval is determined by analyzing the LiDAR backscatter signals for laser wavelengths tuned "on" (λ_{on}) and "off" (λ_{off}) in a molecular absorption peak of the gas under investigation (Browell et al., 1998). The DIAL technique can be used to measure O_3 concentrations above or near a specific location (Browell, 1989). In our DIAL datasets,

https://doi.org/10.5194/acp-2019-634
Preprint. Discussion started: 16 September 2019

the vertical height available was from 0.3 km to 3 km due to the limitations of the signal-to-noise ratio and detection range.

3. Results

3.1. Model performance evaluation

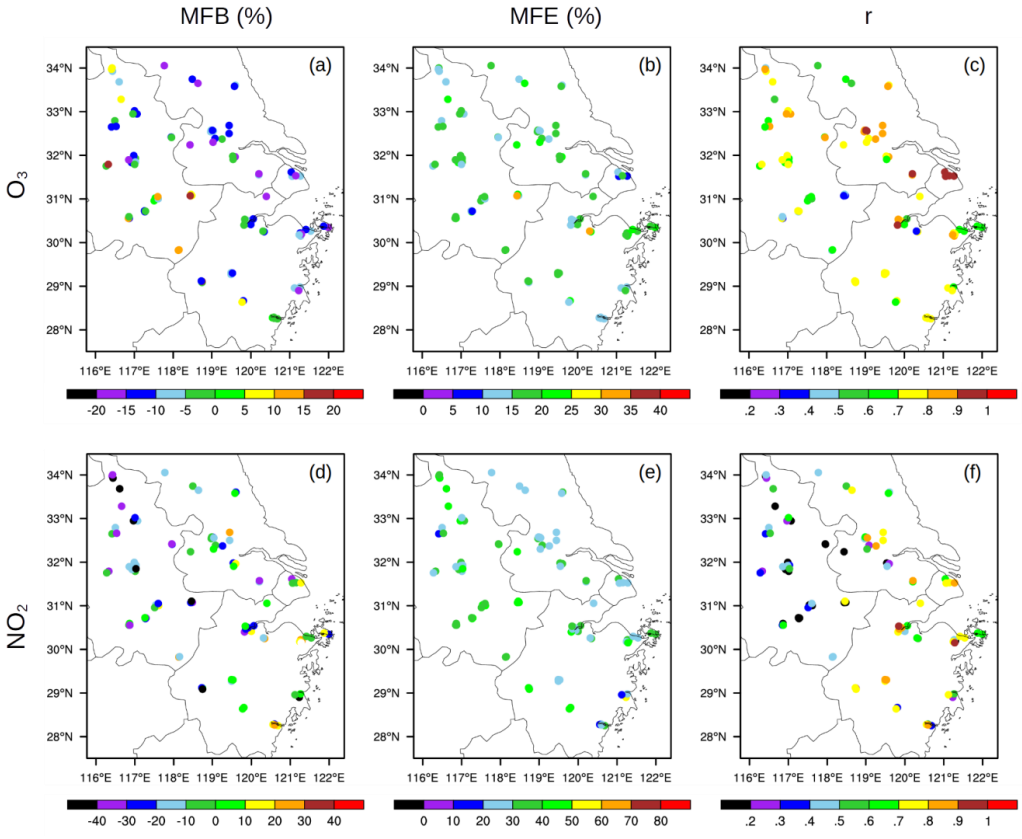

Fig. 2. Comparison of modeled air pollutants concentrations against measurements in 96 monitoring sites over YRD region during August 24–September 6, 2016: Mean fractional bias (MFB), mean fractional error (MFE) and Pearson ' s correlation coefficient (r) of O_3 (a–c) and NO_2 (d–f), respectively.

We first evaluated the overall performance of WRF-Chem for the YRD region by incorporating data from the 96 air quality monitoring sites. Specifically, the maximum daily 8 h (O_3-8h) ozone and daily mean NO_2 concentrations at the surface were used. In general, the model-simulated air pollutant concentrations agreed with the observations. The spatial distributions of MFB and MFE

https://doi.org/10.5194/acp-2019-634
Preprint. Discussion started: 16 September 2019

for O_3 and NO_2 at the 96 observational sites over the YRD region are illustrated in Fig. 2. The results reflected reasonable performance, with MFB and MFE for most of the sites meeting the benchmarks (MFB: 15%; MFE: 35%) proposed by the US Environmental Protection Agency (US EPA; 2007). A scatter plot of MFB/MFE was shown in Fig. S1a,b in the supporting information, further hinting the ability of model in reproducing the observations, which is also reflected by the high correlation between model and observations (Fig. S1c,d in the supporting information). Other model evaluations with satellite retrievals during this period can been seen in our previous study (Ni et al., 2019).

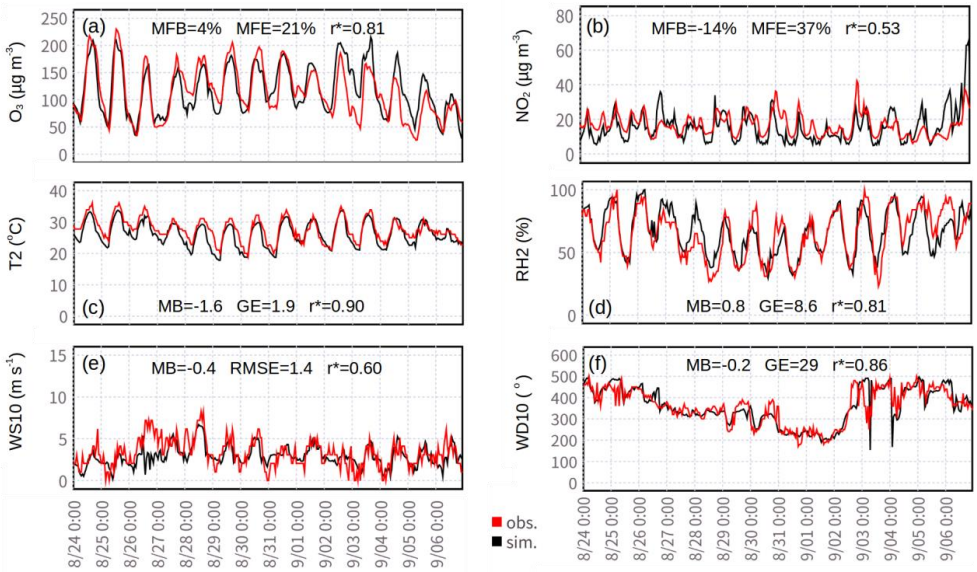

Fig.3. Modeled air pollutants and meteorological parameters compared with measurements at the Hangzhou monitoring site from 24 August to 06 September 2016. Surface concentrations of (a) O_3 and (b) NO_2, (c) temperature at 2 m (T2), (d) relative humidity at 2 m (RH2), (e) wind speed at 10 m (WS10) and (f) wind direction at 10 m (WD10).

Following the overall evaluation of the greater YRD region, the site of Hangzhou was focused on for further analysis, and WRF-Chem simulations of the site's air quality and meteorological conditions were assessed. The time series of hourly simulated and observed air pollutants (O_3, Fig. 3a; NO_2, Fig. 3b) and meteorological factors (T2, Fig. 3c; RH2, Fig. 3d; WS10, Fig. 3e; and WD10,

https://doi.org/10.5194/acp-2019-634
Preprint. Discussion started: 16 September 2019

Fig. 3f) are presented in Fig. 3. All modeled data were statistically significantly correlated with the observed data at the 95% level. Overall, WRF-Chem well represented the observed diurnal variations. For example, the MFB and MFE for both O_3 and NO_2 were near the benchmarks in particular of O_3 levels (MFB/MFE: 4%/21%), and were well below the benchmarks (MFB/MFE: 15%/35%; US EPA; 2007).

For evaluation of meteorological parameters, Emery et al. (2001) proposed benchmarks, including 2 m air temperature (MB ≤ ± 0.5°C, GE ≤ 2.0°C), 10 m wind speed (MB ≤ 0.5 m/s, RMSE ≤ 2.0 m/s) and 10 m wind direction (MB ≤ ± 10°, GE ≤ 30°). McNally (2009) suggested a relaxed benchmark for 2 m temperature (MB ≤ ± 1.0 ℃). In this study, 10 m wind speed and wind direction (Fig. 3e,f) results were well within the proposed limits. The GE of 2 m air temperature (1.9 ℃; Fig. 3c) also satisfied the criteria; however, the MB was slightly higher (−1.6°C), and a slightly high temperature bias was also noted in a previous study (Zhang et al., 2014). Overall, favorable performance was noted for the simulation of meteorological parameters in comparison with observations.

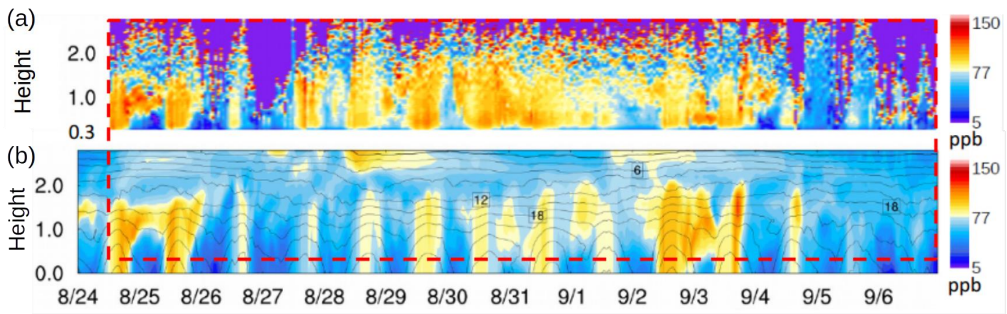

Fig. 4. Upper-level comparison of hourly (a) observed (from differential absorption LiDAR) and (b) simulated O_3 concentrations (ppb) in Hangzhou for 24 August to 06 September 2016. Purple regions in the top panel denote invalid data with a low signal-to-noise ratio. To facilitate direct comparison, the red dashed line indicates the ozone level recorded for the same time periods (starting from 12:00, 24 August) and vertical heights (0.3 – 3 km) in the observations and simulation results.

To further evaluate the ability of the model to reproduce the vertical structure of ozone concentration, the vertical distribution of the modeled O_3 was qualitatively compared with the

https://doi.org/10.5194/acp-2019-634
Preprint. Discussion started: 16 September 2019

DIAL datasets (Fig. 4). The comparison revealed that the model results were consistent with the observations. Diurnal O_3 variations were mainly observed within the planetary boundary layer (approximately <2 km). Notably, the model captured a nocturnal O_3-rich mass, which exhibited an n-shaped distribution in the upper air (approximately 1 km) on 25 August 2016.

3.2. Synoptic weather system

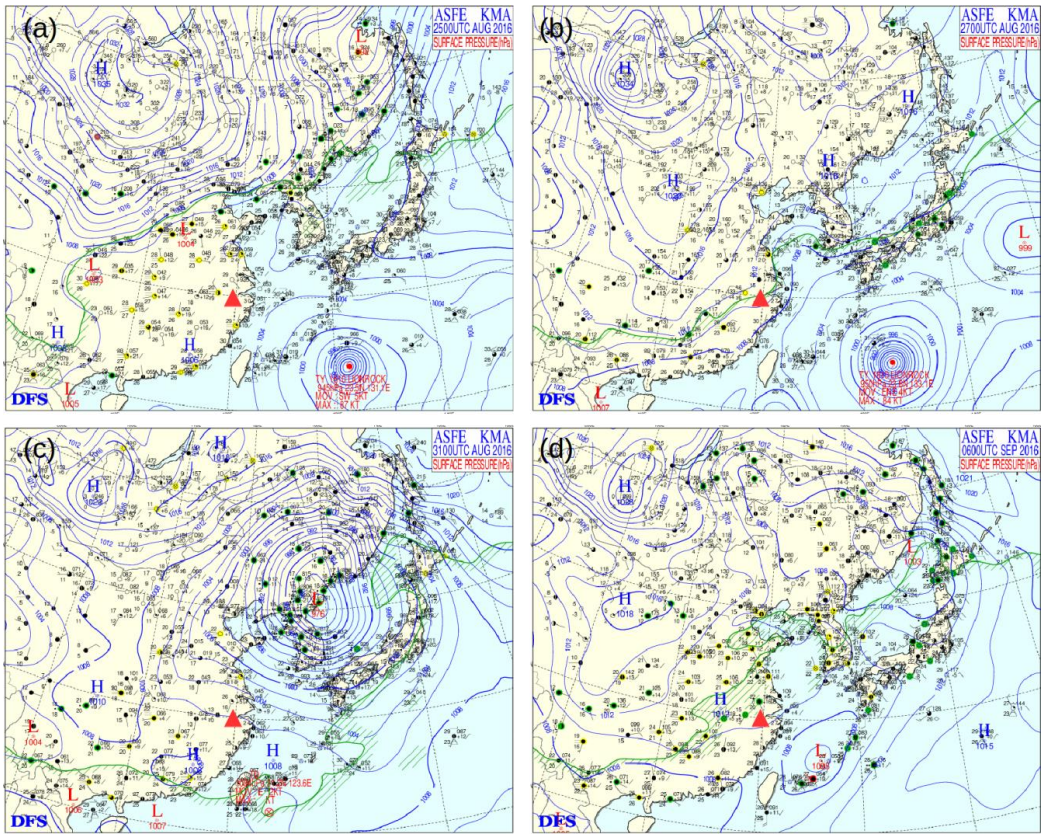

Fig. 5. Tropical cyclone evolution in East Asia during the 2016 G20 summit. Weather charts for four representative periods at 08:00 LST on (a) 25 August, (b) 27 August, (c) 31 August, and (d) 06 September 2016. LST: Local Sidereal Time; H: High-pressure system; L: Low-pressure system. The red triangle denotes the location of Hangzhou. The copyright of map is own to © Korea Meteorological Administration.

Considering the synoptic circulation is closely related to O_3 abundance, four representative surface weather charts obtained from the Korea Meteorological Administration were used to track the tropical cyclone (Fig. 5). In the early stage of the tropical cyclone during 24 and 25 August 2016

https://doi.org/10.5194/acp-2019-634
Preprint. Discussion started: 16 September 2019

(Fig. 5a), strong and uniform high-pressure fields covered vast regions of southeastern China. A tropical cyclone moved northeastward over the East China Sea. In the middle stage (Fig. 5b), the tropical cyclone approached the YRD region, bringing strong north wind fields to this area. The long narrow rain band arrived in Hangzhou (red triangle) on 27 August 2016. In the later stage (Fig. 5c), the cyclone continuously moved toward Japan and eventually hit the land. The tropical high in the YRD region recovered gradually. Finally, the cyclone faded, and a rainstorm appeared over most of the YRD region. This rainstorm continued from approximately 02 through 07 September 2016 (Fig. 5d, for clarity, only the data for 06 September are presented).

3.3. O_3 pollution episode

In Fig. 6, hourly vertical and horizontal O_3 distributions and wind fields in the YRD region are presented for three representative episodes according to the movement of the tropical cyclone. For stagnation days with weak wind fields (i.e., 25 August and 02 September) before or after the tropical cyclone, meteorological conditions were unfavorable for pollutant dispersion. O_3 pollution was more regional and intense, with an hourly peak O_3 concentration of 250 μg m^{-3} below the high layer (2 km) around Hangzhou (Fig. 6a,c). As the cyclone approached (on 27 August), a large belt of O_3-rich mass (>160 μg m^{-3}) appeared in the upwind direction and moved toward Hangzhou under a prevailing north wind field (Fig. 6b). Transboundary pollutant transport played a critical role in these processes, and this finding was consistent with the atmospheric trajectories from North China (Fig. S2). This southward transport of pollutants may supply raw materials for photochemical O_3 generation.

https://doi.org/10.5194/acp-2019-634
Preprint. Discussion started: 16 September 2019

Atmospheric Chemistry and Physics Discussions

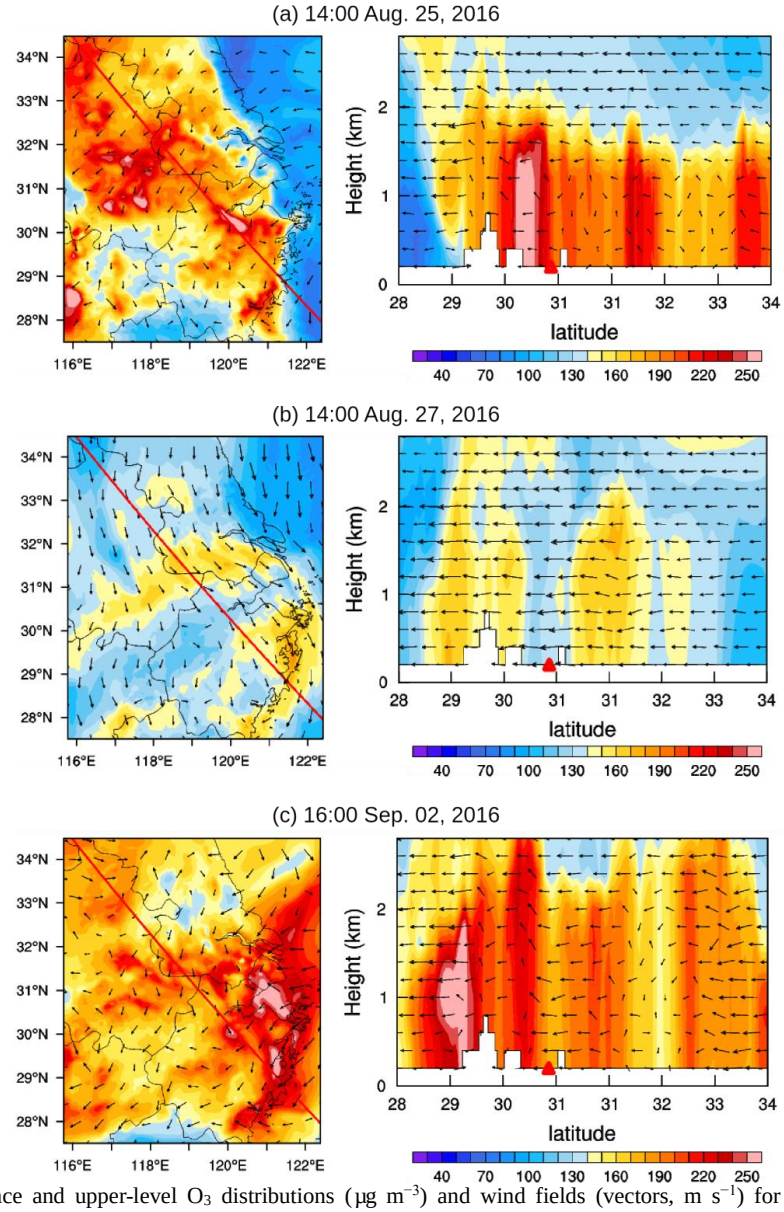

Fig. 6. Surface and upper-level O_3 distributions (μg m^{-3}) and wind fields (vectors, m s^{-1}) for representative episodes. (a) Stagnant weather before the tropical cyclone, (b) pollutant transport when the tropical cyclone approached, and (c) stagnant weather after the cyclone. The red line denotes the cross section line of upper-level O_3 distributions. The red triangle denotes the location of Hangzhou.

https://doi.org/10.5194/acp-2019-634
Preprint. Discussion started: 16 September 2019

3.5. Process analysis of O_3 formation

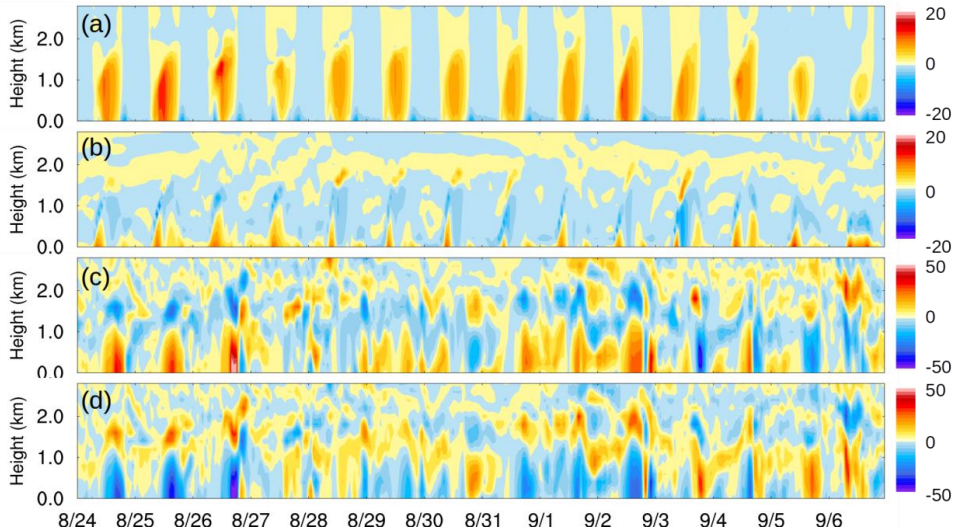

Fig. 7. Hourly variations in the change rate of upper-level O_3 (ppb h^{-1}) resulting from (a) gas chemistry, (b) vertical diffusion, (c) horizontal advection, and (d) vertical advection in Hangzhou.

Four hourly modeled processes indicated the diurnal fluctuations in loops. Gas chemistry resulted in generation of O_3 nearly above the upper-air height of 2 km in the daytime but caused depletion of O_3 at the near-surface height (<0.3 km) in the nighttime (Fig. 7a). O_3 from the upper layer diffused downward to the ground through vertical diffusion during the study period but was significantly higher in the daytime (Fig. 7b). In addition, as indicated in Fig. 8c and d, several dynamic O_3 circulations were observed between the near-surface and upper-air heights during 24 and 25 August and on 02 September 2016. An O_3-rich mass in the lower layer (<1 km) traveled to Hangzhou through horizontal advection, and it was transported from the upper layer to the high layer (approximately 1.5 km) through vertical advection. The mass subsequently reversed and traveled away from Hangzhou in the high layer through horizontal advection in a circular manner. Urban heat island circulations caused the upward and downward flows.

https://doi.org/10.5194/acp-2019-634
Preprint. Discussion started: 16 September 2019

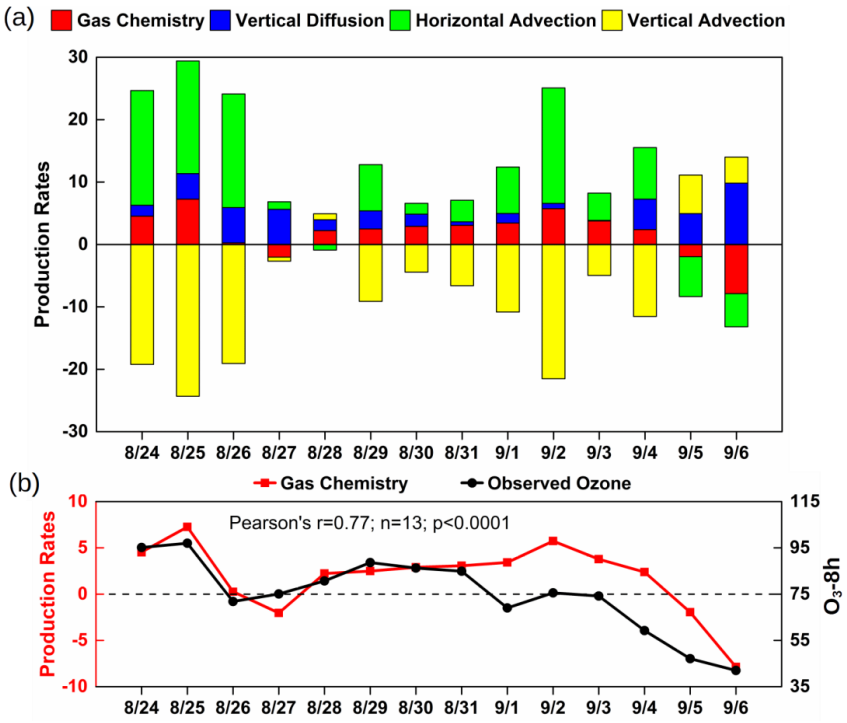

Fig. 8. (a) Daytime mean (08:00–17:00 LST) variations in simulated surface O_3 change rate (ppb h^{-1}; left *y* axis) resulting from gas chemistry, vertical diffusion, and horizontal and vertical advection in Hangzhou. (b) Comparison of daytime mean gas chemistry generation (ppb h^{-1}; left *y* axis) and observed surface-level maximum for daily 8 h concentration of O_3 (O_3-8h; ppb; right *y* axis) in Hangzhou. China's national standard is approximately 75 ppb (160 μg m^{-3}).

The daytime mean variations of O_3 at the ground level resulted from atmospheric processes (Fig. 8a). Quantification of these variations revealed major positive contributions from gas chemistry, vertical diffusion, and horizontal advection to surface O_3 formation, with mean production rates of 1.9, 3.3, and 6.7 ppb h^{-1}, respectively, from 24 August to 06 September 2016. Firstly, the trends between the daytime mean values associated with gas chemistry and observed O_3-8h concentration were consistent (Fig. 8b), indicating a trade-off effect among vertical diffusion and horizontal and vertical advection. High O_3 concentrations (i.e., 25 August 2016 O_3-8h: 98 ppb) were accompanied by prolific generation of gas chemicals. Local chemical generation was found to have large positive correlation (Pearson ' s r = 0.77) with O_3 concentrations. Secondly, vertical diffusion

https://doi.org/10.5194/acp-2019-634
Preprint. Discussion started: 16 September 2019

may have partially compensated for gas chemistry when the chemical reaction rate was relatively low or negative. For example, on 26 and 27 August and 05 and 06 September 2016, most of the vertical diffusion rates were greater than the chemical production rates. The low O_3 episode on these periods mainly resulted from local chemical consumption. Finally, advection processes were essential and integral to air circulation: horizontal advection exerted remarkably positive effects on surface O_3 concentrations in Hangzhou, and vertical advection exerted dispersion effects.

4. Discussion

This study revealed notable background O_3 concentrations in the upper-air layer in the YRD region. Peripheral downdrafts in large-scale cyclone circulation can transport an O_3-rich mass in the upper troposphere or lower stratosphere downward to the surface (Tang et al., 2011; Hsu and Prather, 2014). This type of O_3 intrusion during this period was reported in southeast China (Ni et al., 2019). Based on our results, we inferred that a considerably high background O_3 concentration in the upper air markedly contributed to surface O_3 pollution; this inference agreed (hemispheric background) with the findings of studies conducted in Europe (Wilson et al., 2012) and the United States (Lin et al., 2012, 2015).

We demonstrated that local chemical generation in Hangzhou was enhanced during episodes of high O_3 concentrations before and after the tropical cyclone that occurred during the study period. Chemical generation of O_3 is the net effect of photochemical generation and titration consumption. VOC oxidation (Jenkin et al., 1997; Sillman, 1999) in photochemical reactions provides critical oxidants (i.e., RO_2) that efficiently convert NO to NO_2, resulting in further accumulation of O_3 (Wang et al., 2017). In the present study, downward shortwave flux at the ground level (Fig. S3) was more intense on days with high O_3 concentrations than on those with low O_3 concentrations. This strong solar radiation strengthened O_3 photochemical generation. In addition to the stagnant weather conditions, air subsidence in peripheral circulations of tropical cyclones helps to trap heat and pollutants at the surface (Jiang et al., 2015; Shu et al., 2016). Furthermore, a tropical system with calm, hot–dry weather favors the development of an urban heat island, which causes thermal

https://doi.org/10.5194/acp-2019-634
Preprint. Discussion started: 16 September 2019

circulations as well as the convergence of the surrounding O_3 and its precursors (Lai and Cheng, 2009). The increased temperature also accelerates the photochemical reactions (Narumi et al., 2009; Walcek et al., 1995). In the present study, these enhanced photochemistry processes dominated O_3 chemical generation, resulting in high O_3 concentrations. This result was consistent with the results of a previous field study (Su et al., 2017). Low-level O_3 episodes (i.e., 06 September) in Hangzhou were accompanied by a rain band in the YRD region. Rain band–related cumulus clouds blocked solar radiation, thereby weakening O_3 photochemical generation. Consequently, titration consumption dominated the chemical generation process, resulting in low or negative O_3 chemical production.

5. Conclusions

Changes in O_3 concentrations in Hangzhou during the G20 summit were well represented by the WRF-Chem model. Statistical evaluations of meteorological and chemical parameters suggested that the model system results satisfactorily matched the observed data for both the ground and upper-air levels in MICS-ASIA III. The model results revealed that the O_3 concentrations in Hangzhou were highly related to a tropical cyclone over the East China Sea. Throughout the simulation period, large-scale air mass circulations and energy transport by the tropical cyclone probably caused the high upper-air O_3-rich mass in the horizontal and vertical scales of the YRD region; this phenomenon engendered a negative background O_3 concentration. As the tropical cyclone approached, bringing with it a prevailing north wind component, Hangzhou was affected by pollutant transport from North China. After or before the tropical cyclone, peripheral downdraft or air subsidence produced stable and calm weather, with high pressure and temperature and weak wind, and the urban heat island effect was aggravated. The combination of these conditions enhanced the chemical generation process, resulting in a marked increase in surface O_3 concentrations. Our study provides scientific insight into urban O_3 formation and dispersion under conditions where short-term emission reduction measures had been applied in East China during a tropical cyclone event.

https://doi.org/10.5194/acp-2019-634
Preprint. Discussion started: 16 September 2019

Author contribution

Kun Luo and Xiang Gao designed the experiments. Fei Jiang, Huang Cheng, Jian-ren Fan, Joshua S Fu and Chang-hong Chen edit the manuscript. Zhi-zhen Ni and Yang Gao prepared the manuscript with contributions from all co-authors

Acknowledgments

This work was financially supported by special funds from the Ministry of Environmental Protection of China (No. 201409008-4) and the Zhejiang Provincial Key Science and Technology Project for Social Development (No. 2014C03025). We would like to thank the US National Oceanic and Atmospheric Administration for its technical support in WRF-Chem modeling. High-resolution emission inventories were provided by the Institute of Environmental Science, Shanghai, China, and the official documents of emission control policies were obtained from the Hangzhou Environmental Monitoring Center.

Reference

Browell, E.V., Ismail, S., Grant, W.B.: Differential absorption lidar (DIAL) measurements from air and space, Appl. Phys. B Lasers Opt, 67, 399–410, https://doi.org/10.1007/s003400050523, 1998.

Browell, E. V.: Differential Absorption Lidar Sensing of Ozone, Proc. IEEE, 77, 419–432, https://doi.org/10.1109/5.24128, 1989

Brown, J.F., Loveland, T.R., Merchant, J.W., Reed, B.C., Ohlen, D.O.: Using Multisource Data in Global Land-Cover Characterization - Concepts, Requirements, and Methods, Photogramm. Eng. Remote Sensing, 59, 977–987, 1993.

Calfapietra, C., Morani, A., Sgrigna, G., Di Giovanni, S., Muzzini, V., Pallozzi, E., Guidolotti, G., Nowak, D., Fares, S.: Removal of Ozone by Urban and Peri-Urban Forests: Evidence from Laboratory, Field, and Modeling Approaches, J. Environ. Qual, 45, 224, https://doi.org/10.2134/jeq2015.01.0061, 2016.

Cheng, W.L., Lai, L.W., Den, W., Wu, M.T., Hsueh, C.A., Lin, P.L., Pai, C.L., Yan, Y.L.: The relationship between typhoons ' peripheral circulation and ground-level ozone concentrations in central Taiwan, Environ. Monit. Assess, 186, 791–804, https://doi.org/10.1007/s10661-013-3417-7, 2014.

https://doi.org/10.5194/acp-2019-634
Preprint. Discussion started: 16 September 2019

Emery, C., Tai, E., Yarwood, G.: Enhanced meteorological modeling and performance evaluation for two Texas episodes, International Corp (Ed.), Report to the Texas Natural Resources Conservation Commission, p.b.E (2001) [Novato, CA.], 2001

Emmons, L.K., Walters, S., Hess, P.G., Lamarque, J.-F., Pfister, G.G., Fillmore, D., Granier, C., Guenther, A., Kinnison, D., Laepple, T., Orlando, J., Tie, X., Tyndall, G., Wiedinmyer, C., Baughcum, S.L., Kloster, S.: Description and evaluation of the Model for Ozone and Related chemical Tracers, version 4 (MOZART-4), Geosci. Model Dev., 3, 43–67, https://doi.org/10.5194/gmd-3-43-2010, 2010.

Friedl, M. ., McIver, D. ., Hodges, J. C. ., Zhang, X. ., Muchoney, D., Strahler, A. ., Woodcock, C. ., Gopal, S., Schneider, A., Cooper, A., Baccini, A., Gao, F. and Schaaf, C.: Global land cover mapping from MODIS: algorithms and early results, Remote Sens. Environ., 83(12), 287–302, https://doi.org/10.1016/S0034-4257(02)00078-0, 2002.

Gao, J., Zhu, B., Xiao, H., Kang, H., Hou, X., Shao, P.: A case study of surface ozone source apportionment during a high concentration episode, under frequent shifting wind conditions over the Yangtze River Delta, China, Sci. Total Environ, 544, 853–863, https://doi.org/10.1016/j.scitotenv.2015.12.039, 2016.

Gonçalves, M., Jiménez-Guerrero, P., Baldasano J.M.: Contribution of atmospheric processes affecting the dynamics of air pollution in South-Western Europe during a typical summertime photochemical episode, Atmos. Chem. Phys, 9, 849–864, https://doi.org/10.5194/acp-9-849-2009, 2009.

Grell, G.A., Peckham, S.E., Schmitz, R., McKeen, S.A., Frost, G., Skamarock, W.C., Eder, B. Fully coupled "online" chemistry within the WRF model, Atmos. Environ., 39, 6957–6975, https://doi.org/10.1016/j.atmosenv.2005.04.027, 2005.

Grell, G., Baklanov, A.: Integrated modeling for forecasting weather and air quality: A call for fully coupled approaches, Atmos. Environ., 45, 6845–6851, https://doi.org/10.1016/j.atmosenv.2011.01.017, 2011.

Ha, S., Hu, H., Roussos-Ross, D., Haidong, K., Roth, J., Xu, X.: The effects of air pollution on adverse birth outcomes, Environ. Res., 134, 198–204, https://doi.org/10.1016/j.envres.2014.08.002, 2014.

Hsu, J., Prather, M.J.: Is the residual vertical velocity a good proxy for stratosphere-troposphere exchange of ozone?, Geophys. Res. Lett., 41, 9024–9032, https://doi.org/10.1002/2014GL061994, 2014.

Huang, J.P., Fung, J.C.H., Lau, A.K.H., Qin, Y.: Numerical simulation and process analysis of typhoon-related ozone episodes in Hong Kong, J. Geophys. Res. D Atmos., 110, 1–17, https://doi.org/10.1029/2004JD004914, 2005.

Huang, C., Chen, C. H., Li, L., Cheng, Z., Wang, H. L., Huang, H. Y., Streets, D. G., Wang, Y. J., Zhang, G. F. and Chen, Y. R.: Emission inventory of anthropogenic air pollutants and VOC species in the Yangtze River Delta region, China, Atmos. Chem. Phys., https://doi.org/10.5194/acp-11-4105-2011, 2011.

Hung, C.H., LouoC, K.: Relationships between Ambient Ozone Concentration Changes in Southwestern Taiwan and Invasion Tracks of Tropical Typhoons, Adv. Meteorol., https://doi.org/10.1155/2015/402976, 2015.

Jenkin, M. E., Saunders, S. M. and Pilling, M. J.: The tropospheric degradation of volatile organic compounds: A protocol for mechanism development, Atmos. Environ., 31(1), 81 – 104, https://doi.org/10.1016/S1352-2310(96)00105-7, 1997.

Jiang, F., Zhou, P., Liu, Q., Wang, T., Zhuang, B., Wang, X.: Modeling tropospheric ozone formation over East China in springtime, J. Atmos. Chem., 69, 303 – 319, https://doi.org/10.1007/s10874-012-9244-3, 2012.

Jiang, Y.C., Zhao, T.L., Liu, J., Xu, X.D., Tan, C.H., Cheng, X.H., Bi, X.Y., Gan, J.B., You, J.F., Zhao, S.Z.: Why does surface ozone peak before a typhoon landing in southeast China?, Atmos. Chem. Phys., 15, 13331 – 13338, https://doi.org/10.5194/acp-15-13331-2015, 2015.

Jones, S.L., Creighton, G.A., Kuchera, E.L., Rentschler, S.A.: Adapting WRF-CHEM GOCART for Fine-Scale Dust Forecasting, in: AGU Fall Meeting Abstracts, p. 6., 2011.

Kalnay, E., M. Kanamitsu, R. Kistler, W. Collins, D. Deaven, L. Gandin, M. Iredell, S. Saha, G. White, J. Woollen, Y. Zhu, M. Chelliah, W. Ebisuzaki, W. Higgins, J. Janowiak, K.C. Mo, C. Ropelewski, J. Wang, A. Leetmaa, R. Reynolds, R. Jenne, and D. Joseph: The NCEP/NCAR 40-Year Reanalysis Project, Bull. Amer. Meteor. Soc., 77, 437 – 472, https://doi.org/10.1175/1520-0477(1996)077<0437:TNYRP>2.0.CO;2, 1996.

Kheirbek, I., Wheeler, K., Walters, S., Kass, D., Matte, T.: PM2.5 and ozone health impacts and disparities in New York City: Sensitivity to spatial and temporal resolution, Air Qual. Atmos. Heal., 6, 473 – 486, https://doi.org/10.1007/s11869-012-0185-4, 2013.

Knote, C., Tuccella, P., Curci, G., Emmons, L., Orlando, J.J., Madronich, S., Baró, R., Jiménez-Guerrero, P., Luecken, D., Hogrefe, C., Forkel, R., Werhahn, J., Hirtl, M., Pérez, J.L., San José, R., Giordano, L., Brunner, D., Yahya, K., Zhang, Y.: Influence of the choice of gas-phase mechanism on predictions of key gaseous pollutants during the AQMEII phase-2 intercomparison, Atmos. Environ., 115, 553 – 568, https://doi.org/10.1016/j.atmosenv.2014.11.066, 2015.

Lai, L. W. and Cheng, W. L.: Air quality influenced by urban heat island coupled with synoptic weather patterns, Sci. Total Environ., 407(8), 2724 – 2733, https://doi.org/10.1016/j.scitotenv.2008.12.002, 2009.

Landry, J.S., Neilson, E.T., Kurz, W.A., Percy, K.E.: The impact of tropospheric ozone on landscape-level merchantable biomass and ecosystem carbon in Canadian forests, Eur. J. For. Res., 132, 71–81, https://doi.org/10.1007/s10342-012-0656-z, 2013.

Lelieveld, J., Evans, J.S., Fnais, M., Giannadaki, D., Pozzer, A.: The contribution of outdoor air pollution sources to premature mortality on a global scale, Nature, 525, 367–71, https://doi.org/10.1038/nature15371, 2015.

Li, J., Nagashima, T., Kong, L., Ge, B., Yamaji, K., Fu, J. S., Wang, X., Fan, Q., Itahashi, S., Lee, H.-J., Kim, C.-H., Lin, C.-Y., Zhang, M., Tao, Z., Kajino, M., Liao, H., Li, M., Woo, J.-H., Kurokawa, J.-I., Wu, Q., Akimoto, H., Carmichael, G. R., and Wang, Z.: Model evaluation and inter-comparison of surface-level ozone and relevant species in East Asia in the context of MICS-Asia phase III Part I: overview, Atmos. Chem. Phys. Discuss., https://doi.org/10.5194/acp-2018-1283, in review, 2019.

Li, L., Chen, C. H., Fu, J. S., Huang, C., Streets, D. G., Huang, H. Y., Zhang, G. F., Wang, Y. J., Jang, C. J., Wang, H. L., Chen, Y. R. and Fu, J. M.: Air quality and emissions in the Yangtze River Delta, China, Atmos. Chem. Phys., https://doi.org/10.5194/acp-11-1621-2011, 2011.

Li, M., Song, Y., Huang, X., Li, J., Mao, Y., Zhu, T., Cai, X. and Liu, B.: Improving mesoscale modeling using satellite-derived land surface parameters in the Pearl River Delta region, China, J. Geophys. Res. Atmos., 119(11), 6325–6346, https://doi.org/10.1002/2014JD021871, 2014.

Li, M., Zhang, Q., Kurokawa, J.-I., Woo, J.-H., He, K., Lu, Z., Ohara, T., Song, Y., Streets, D.G., Carmichael, G.R., Cheng, Y., Hong, C., Huo, H., Jiang, X., Kang, S., Liu, F., Su, H., Zheng, B.: MIX: a mosaic Asian anthropogenic emission inventory under the international collaboration framework of the MICS-Asia and HTAP, Atmos. Chem. Phys., 17, 935–963, https://doi.org/10.5194/acp-17-935-2017, 2017.

Lin, M., Fiore, A.M., Cooper, O.R., Horowitz, L.W., Langford, A.O., Levy, H., Johnson, B.J., Naik, V., Oltmans, S.J., Senff, C.J.: Springtime high surface ozone events over the western United States: Quantifying the role of stratospheric intrusions, J. Geophys. Res. Atmos., 117, https://doi.org/10.1029/2012JD018151, 2012.

Lin, M., Fiore, A.M., Horowitz, L.W., Langford, A.O., Oltmans, S.J., Tarasick, D., Rieder, H.E.: Climate variability modulates western US ozone air quality in spring via deep stratospheric intrusions, Nat. Commun., 6, 7105, https://doi.org/10.1038/ncomms8105, 2015.

Liu, Y., Li, L., An, J., Huang, L., Yan, R., Huang, C., Wang, H., Wang, Q., Wang, M. and Zhang, W.: Estimation of biogenic VOC emissions and its impact on ozone formation over the Yangtze River Delta region, China, Atmos. Environ., https://doi.org/10.1016/j.atmosenv.2018.05.027, 2018.

McNally DE: 12 km MM5 performance goals, Presentation to the Ad-hov Meteorology Group, 2009.

Monks, P.S., Archibald, A.T., Colette, A., Cooper, O., Coyle, M., Derwent, R., Fowler, D., Granier, C., Law, K.S., Mills, G.E., Stevenson, D.S., Tarasova, O., Thouret, V., von Schneidemesser, E., Sommariva, R., Wild, O., Williams, M.L.: Tropospheric ozone and its precursors from the urban to the global scale from air quality to short-lived climate forcer, Atmos. Chem. Phys., 15, 8889–8973, https://doi.org/10.5194/acp-15-8889-2015, 2015.

Nagashima, T., Sudo, K., Akimoto, H., Kurokawa, J., Ohara, T., 2017. Long-term change in the source contribution to surface ozone over Japan. Atmos. Chem. Phys. 17, 8231–8246, https://doi.org/10.5194/acp-17-8231-2017

Narumi, D., Kondo, A. and Shimoda, Y.: The effect of the increase in urban temperature on the concentration of photochemical oxidants, Atmos. Environ., 43(14), 2348–2359, https://doi.org/10.1016/j.atmosenv.2009.01.028, 2009.

Ni, Z. zhen, Luo, K., Zhang, J. xi, Feng, R., Zheng, H. xin, Zhu, H. ran, Wang, J. fan, Fan, J. ren, Gao, X. and Cen, K. fa: Assessment of winter air pollution episodes using long-range transport modeling in Hangzhou, China, during World Internet Conference, 2015, in Environmental Pollution, vol. 236, pp. 550–561., 2018.

Ni, Z. zhen, Luo, K., Gao, X., Gao, Y., Fan, J. ren, Fu, Joshua S. Cen, C.,: Exploring the stratospheric source of ozone pollution over China during the 2016 Group of Twenty summit, 2019, Atmospheric Pollution Research, https://doi.org/10.1016/j.apr.2019.02.010

Paoletti, E., De Marco, A., Beddows, D.C.S., Harrison, R.M., Manning, W.J.: Ozone levels in European and USA cities are increasing more than at rural sites, while peak values are decreasing, Environ. Pollut., 192, 295–299, https://doi.org/10.1016/j.envpol.2014.04.040, 2014.

Shi, C., Wang, S., Liu, R., Zhou, R., Li, D., Wang, W., Li, Z., Cheng, T., Zhou, B.: A study of aerosol optical properties during ozone pollution episodes in 2013 over Shanghai, China, Atmos. Res., 153, 235–249, https://doi.org/10.1016/j.atmosres.2014.09.002, 2015.

Shu, L., Xie, M., Wang, T., Chen, P., Han, Y., Li, S., Zhuang, B., Li, M., Gao, D.: Integrated studies of a regional ozone pollution synthetically affected by subtropical high and typhoon system in the Yangtze River Delta region, China, Atmos. Chem. Phys. Discuss., 0, 1–32, https://doi.org/10.5194/acp-2016-581, 2016.

Sillman, S.: The relation between ozone, NO(x) and hydrocarbons in urban and polluted rural environments, Atmos. Environ., 33(12), 1821–1845, https://doi.org/10.1016/S1352-2310(98)00345-8, 1999.

Stauffer, D.R., Seaman, N.L., Binkowski, F.S.: Use of Four-Dimensional Data Assimilation in a Limited-Area Mesoscale Model Part II: Effects of Data Assimilation within the Planetary Boundary Layer, Mon. Weather Rev., https://doi.org/10.1175/1520-0493(1991)119<0734:UOFDDA>2.0.CO;2, 1991.

Su, W., Liu, C., Hu, Q., Fan, G., Xie, Z., Huang, X., Zhang, T., Chen, Z., Dong, Y., Ji, X., Liu, H., Wang, Z., Liu, J.: Characterization of ozone in the lower troposphere during the 2016 G20 conference in Hangzhou, Sci. Rep., 7, 17368, https://doi.org/10.1038/s41598-017-17646-x, 2017.

Tang, G., Li, X., Wang, Y., Xin, J., Ren, X.: Surface ozone trend details and interpretations in Beijing, 2001 – 2006, Atmos. Chem. Phys., 8813 – 8823, https://doi.org/10.5194/acpd-9-8159-2009, 2009.

Tang, G., Wang, Y., Li, X., Ji, D., Hsu, S., Gao, X.: Spatial-temporal variations in surface ozone in Northern China as observed during 2009-2010 and possible implications for future air quality control strategies, Atmos. Chem. Phys., 12, 2757 – 2776, https://doi.org/10.5194/acp-12-2757-2012, 2012.

Tang, G., Zhu, X., Xin, J., Hu, B., Song, T., Sun, Y., Wang, L., Cheng, M., Li, X., Wang, Y., Zhang, J., Chao, N., Kong, L., Li, X.: Modelling study of boundary-layer ozone over northern China - Part I: Ozone budget in summer, Atmos. Res., 187, 128 – 137, https://doi.org/10.1016/j.atmosres.2016.10.017, 2017a.

Tang, Q., Prather, M.J., Hsu, J.: Stratosphere-troposphere exchange ozone flux related to deep convection, Geophys. Res. Lett., 38, https://doi.org/10.1029/2010GL046039, 2011.

Teixeira, E., Fischer, G., van Velthuizen, H., van Dingenen, R., Dentener, F., Mills, G., Walter, C., Ewert, F.: Limited potential of crop management for mitigating surface ozone impacts on global food supply, Atmos. Environ., 45, 2569 – 2576, https://doi.org/10.1016/j.atmosenv.2011.02.002, 2011.

Tie, X., Geng, F., Guenther, A., Cao, J., Greenberg, J., Zhang, R., Apel, E., Li, G., Weinheimer, A., Chen, J., Cai, C.: Megacity impacts on regional ozone formation: Observations and WRF-Chem modeling for the MIRAGE-Shanghai field campaign, Atmos. Chem. Phys., 13, 5655 – 5669, https://doi.org/10.5194/acp-13-5655-2013, 2013.

USEPA: Guidance on the Use of Models and Other Analyses for Demonstrating Attainment of Air Quality Goals for Ozone, PM2.5 and Regional Haze, EPA-454/B-07e002. USEPA, 2007

von Schneidemesser, E., Coates, J., Denier van der Gon, H.A.C., Visschedijk, A.J.H., Butler, T.M.: Variation of the NMVOC speciation in the solvent sector and the sensitivity of modelled tropospheric ozone, Atmos. Environ., 135, 59 – 72, https://doi.org/10.1016/j.atmosenv.2016.03.057, 2016.

Walcek, C. J., Yuan, H.-H., Walcek, C. J. and Yuan, H.-H.: Calculated Influence of Temperature-Related Factors on Ozone Formation Rates in the Lower Troposphere, J. Appl. Meteorol., 34(5), 1056 – 1069, https://doi.org/10.1175/1520-0450(1995)034<1056:CIOTRF>2.0.CO;2, 1995.

Wang, S., Xing, J., Chatani, S., Hao, J., Klimont, Z., Cofala, J., Amann, M.: Verification of anthropogenic emissions of China by satellite and ground observations, Atmos. Environ., 45, 6347 – 6358, https://doi.org/10.1016/j.atmosenv.2011.08.054, 2011.

Wang, T.J., Lam, K.S., Xie, M., Wang, X.M., Carmichael, G., Li, Y.S.: Integrated studies of a photochemical smog episode in Hong Kong and regional transport in the Pearl River Delta of China, Tellus, Ser. B Chem. Phys. Meteorol., 58, 31 – 40, https://doi.org/10.1111/j.1600-0889.2005.00172.x, 2006.

Wang, T., Xue, L., Brimblecombe, P., Lam, Y. F., Li, L. and Zhang, L.: Ozone pollution in China: A review of concentrations, meteorological influences, chemical precursors, and effects, Sci. Total Environ., 575, 1582 – 1596, https://doi.org/10.1016/j.scitotenv.2016.10.081, 2017.

Wang, Y., Hu, B., Tang, G., Ji, D., Zhang, H., Bai, J., Wang, X., Wang, Y.: Characteristics of ozone and its precursors in Northern China: A comparative study of three sites, Atmos. Res., 132 – 133, 450 – 459, https://doi.org/10.1016/j.atmosres.2013.04.005, 2013.

Wang, Y.H., Hu, B., Ji, D.S., Liu, Z.R., Tang, G.Q., Xin, J.Y., Zhang, H.X., Song, T., Wang, L.L., Gao, W.K., Wang, X.K., Wang, Y.S.: Ozone weekend effects in the Beijing-Tianjin-Hebei metropolitan area, China, Atmos. Chem. Phys., 14, 2419 – 2429, https://doi.org/10.5194/acp-14-2419-2014, 2014.

Wilson, R.C., Fleming, Z.L., Monks, P.S., Clain, G., Henne, S., Konovalov, I.B., Szopa, S., Menut, L.: Have primary emission reduction measures reduced ozone across Europe? An analysis of European rural background ozone trends 1996-2005, Atmos. Chem. Phys., 12, 437 – 454, https://doi.org/10.5194/acp-12-437-2012, 2012.

Xie, M., Zhu, K., Wang, T., Yang, H., Zhuang, B., Li, S., Li, M., Zhu, X., Ouyang, Y.: Application of photochemical indicators to evaluate ozone nonlinear chemistry and pollution control countermeasure in China, Atmos. Environ., 99, 466 – 473, https://doi.org/10.1016/j.atmosenv.2014.10.013, 2014.

Xue, L.K., Wang, T., Gao, J., Ding, A.J., Zhou, X.H., Blake, D.R., Wang, X.F., Saunders, S.M., Fan, S.J., Zuo, H.C., Zhang, Q.Z., Wang, W.X.: Ground-level ozone in four Chinese cities: Precursors, regional transport and heterogeneous processes, Atmos. Chem. Phys., 14, 13175 – 13188, https://doi.org/10.5194/acp-14-13175-2014, 2014.

https://doi.org/10.5194/acp-2019-634
Preprint. Discussion started: 16 September 2019

Zhang, B.N., Kim Oanh, N.T.: Photochemical smog pollution in the Bangkok Metropolitan Region of Thailand in relation to O3 precursor concentrations and meteorological conditions, Atmos. Environ., 36, 4211–4222, https://doi.org/10.1016/S1352-2310(02)00348-5, 2002.

Zhang, H., Chen, G., Hu, J., Chen, S.H., Wiedinmyer, C., Kleeman, M., Ying, Q.: Evaluation of a seven-year air quality simulation using the Weather Research and Forecasting (WRF)/Community Multiscale Air Quality (CMAQ) models in the eastern United States, Sci. Total Environ., 473–474, 275–285, https://doi.org/10.1016/j.scitotenv.2013.11.121, 2014.